nature physics

SUPPLEMENTARY INFORMATION

DOI: 10.1038/NPHYS4009

In the format provided by the authors and unedited.

Generalized non-reciprocity in an optomechanical circuit via synthetic magnetism and reservoir engineering

Kejie Fang,[1,2] Jie Luo,[1,2] Matthew H. Matheny,[1,3] Anja Metelmann,[4,5] Florian Marquardt,[6,7] Aashish A. Clerk,[4] and Oskar Painter[1,2]

[1] *Kavli Nanoscience Institute, California Institute of Technology, Pasadena, California 91125, USA*
[2] *Institute for Quantum Information and Matter and Thomas J. Watson, Sr., Laboratory of Applied Physics, California Institute of Technology, Pasadena, California 91125, USA*
[3] *Department of Physics, California Institute of Technology, Pasadena, California 91125, USA*
[4] *Department of Physics, McGill University, 3600 rue University, Montréal, Quebec H3A 2T8, Canada*
[5] *Department of Electrical Engineering, Princeton University, Princeton, New Jersey 08544, USA*
[6] *Max Planck Institute for the Science of Light, Günther-Scharowsky-Straße 1/Bau 24, D-91058 Erlangen, Germany*
[7] *Institute for Theoretical Physics, Department of Physics, Universität Erlangen-Nürnberg, 91058 Erlangen*

I. DEVICE FABRICATION AND CHARACTERIZATION

A. Device fabrication and atomic force microscope nano-oxidation tuning

The devices were fabricated from a silicon-on-insulator wafer with a silicon device layer thickness of 220 nm and buried-oxide layer thickness of 2 μm. The device geometry was defined by electron-beam lithography followed by inductively coupled plasma reactive ion etching to transfer the pattern through the 220 nm silicon device layer. The devices were then undercut using an HF:H_2O solution to remove the buried oxide layer and cleaned using a piranha etch.

After device fabrication, we used an atomic force microscope to draw nanoscale oxide patterns on the silicon device surface. This process modifies the optical and mechanical cavity frequencies in a controllable and independent way with the appropriate choice of oxide pattern. The nano-oxidation process was carried out using an Asylum MFP-3D atomic force microscope and conductive diamond tips (NaDiaProbes) in an environment with relative humidity of 48%. The tip was biased at a voltage of −11.5 V, scanned with a velocity of 100 nm/s, and run in tapping mode with an amplitude of 10 nm. The unpassivated silicon device surface was grounded.

B. Optical transmission coefficient measurement

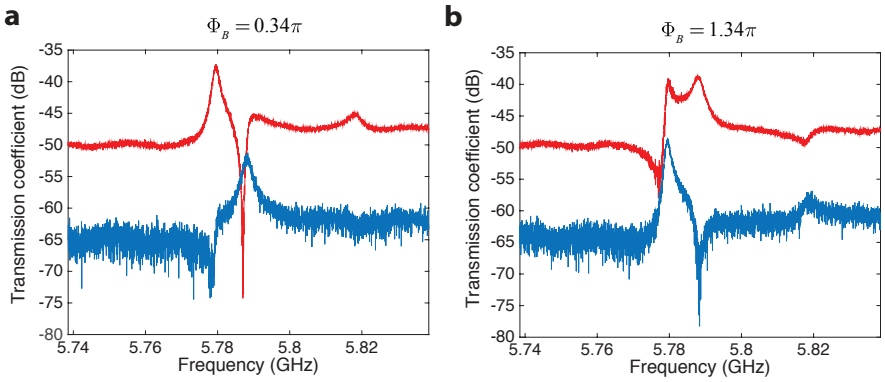

FIG. S1. **a** Microwave signal power transmission through the optomechanical circuit for forward (right-propagation; blue) and backward (left-propagation; blue curve) directions, with flux set to $\Phi_B = 0.34\pi$ and cavity photon number $n_{cL} = 1000$ and $n_{cR} = 1420$. **b** Same as **a** but with $\Phi_B = 1.34\pi$.

To measure the optical power transmission through the optomechanical circuit we used a vector network analyzer (VNA). The VNA outputs a microwave tone from port 1 with frequency $\omega_{\rm mod}$ to an electro-optic modulator which modulates the optical pump to generate an optical sideband corresponding to the optical probe. In the case of a

blue-detuned pump from the optical cavity resonance, the probe field corresponds to the lower sideband (selected by the filtering properties of the cavity itself). Both the optical probe and pump are launched into one optomechanical cavity in the circuit. At the other cavity, the transmitted optical probe combines with a second pump and the beating of the two is detected by a high-speed photodetector (both the first and second pump beams are from the same laser source, and thus phase coherent). The photocurrent signal from the photodetector is sent into port 2 of the VNA to measure the microwave signal transmission coefficient T_μ. Fig. S1 shows $|T_\mu|^2$ for forward (right-propagating; blue curve) and backward (left-propagating; red curve) directions through the optomechanical circuit as a function of the modulation frequency $\omega_{\rm mod}$. In Fig. S1a the synthetic flux value is locked to $\Phi_{\rm B} = 0.34\pi$ whereas in Fig. S1b $\Phi_{\rm B} = 1.34\pi$. In both flux settings the optical pumping levels were such that the left and right cavity photon numbers were $n_{cL} = 1000$ and $n_{cR} = 1420$, respectively. This is the raw transmission data corresponding to the normalized transmission ratio shown in Figs. 3b and 3c of the main text.

While absolute optical transmission is not directly measured, the ratio of the optical transmission coefficients for forward and backward propagation can be obtained from the normalized microwave signal transmission coefficient $\bar{T}_\mu$,

$$|T_{\rm L\to R}/T_{\rm R\to L}|^2 = |\bar{T}_{\mu R}/\bar{T}_{\mu L}|^2, \tag{S1}$$

where $|\bar{T}_\mu|^2$ is normalized using the value of $|T_\mu|^2$ away from all mechanical resonances to remove all the external asymmetry in the experimental setup for left and right propagation paths. These external asymmetries include modulator efficiency, cable/fiber loss, etc. In our analysis the normalization level is the average value of $|T_\mu|^2$ in the frequency range of 5.74-5.76 GHz. To be clear, the reason this calibration is necessary is because we don't actually physically swap the source and detector in our measurements. Rather, for the left-to-right transmission path we have one modulator on the left side which generates the probe tone and one detector on the right side which measures the transmission through to the right side. When we measure right-to-left transmission we have a different modulator on the right side to generate the probe tone and a different detector on the left side to detect the transmitted probe. If the modulator on the left side is different from the modulator on the right side, then for the same microwave drive that excites the modulators we would get different a different optical probe power in the sidebands of the pump. Similarly if the left and right detectors have different efficiencies then they would produce a different photocurrent for the same transmitted optical probe power. Since we measure in practice the ratio of the microwave drive to the detected microwave photocurrent, this could cause an inherent asymmetry in the measured transmission for left-to-right and right-to-left transmission even if the *optical* transmission was perfectly symmetric.

C. Device characterization

To determine the components of optical cavity loss (intrinsic decay rate $\kappa_{\rm i}$, external waveguide-to-cavity coupling $\kappa_{\rm e}$, total cavity decay rate κ) of both the left and right optical cavities we used a pump-probe scheme similar to that used to measure the nonreciprocity of the optomechanical circuit. The pump beam in this case, however, is set to be very weak so as to not resonantly excite the mechanics as the probe signal is swept across the optical cavity resonance. The cavity scans are plotted in Fig. S2a and S2b for the left and right cavities, respectively. We fit the phase response curves and get $\kappa_{\rm iL(R)}/2\pi = 0.29$ (0.31) GHz, $\kappa_{\rm eL(R)}/2\pi = 0.74$ (0.44) GHz, and $\kappa_{\rm L(R)}/2\pi = 1.03$ (0.75) GHz. The intrinsic and external optical cavity rates are used to determine the intra-cavity photon number for a given optical pump power (specified at the input to the cavity).

Thermal mechanical spectra of the two cavities are measured with a weak blue-detuned optical pump so as to avoid back-action; a single pump is used for each of the left and right cavity measurements. The reflected pump light from the cavity contains modulation sidebands from the thermal mechanical motion, which upon detection with a high-speed photodetector creates a photocurrent with the thermal motion of the mechanical cavity modes imprinted on it. Since the mechanical modes can be hybridized between left-cavity, right-cavity, and waveguide modes, a measurement with the left-side pump produces a local measurement of the cavity modes as measured by the localized left optical cavity mode, and similarly for the right-side pump and cavity. The intrinsic decay rate of the mechanical modes is inferred from the linewidth of the Lorentzian mechanical spectrum.

Measurements of the mechanical mode spectra were performed both before and after the cavities were nano-oxidized to tune their localized optical and mechanical modes into resonance. Measurements prior to nano-oxidation allowed us to determine the local (left and right) mechanical and optical cavity mode properties (i.e., the bare, uncoupled mode properties). Knowing the left and right cavity mode properties from independent measurements allowed us to fit with fewer fitting parameters the measured forward and backward transmission curves of the hybridized cavities presented in the main article text. Note that after nano-oxidation the left and right optical cavity modes were only very weakly hybridized so as to maintain their left-cavity and right-cavity character. The mechanical modes were tuned to be strongly hybdridized as evidenced in Fig. 2f of the main text. Figures S2c and S2d show the measured linewidth of

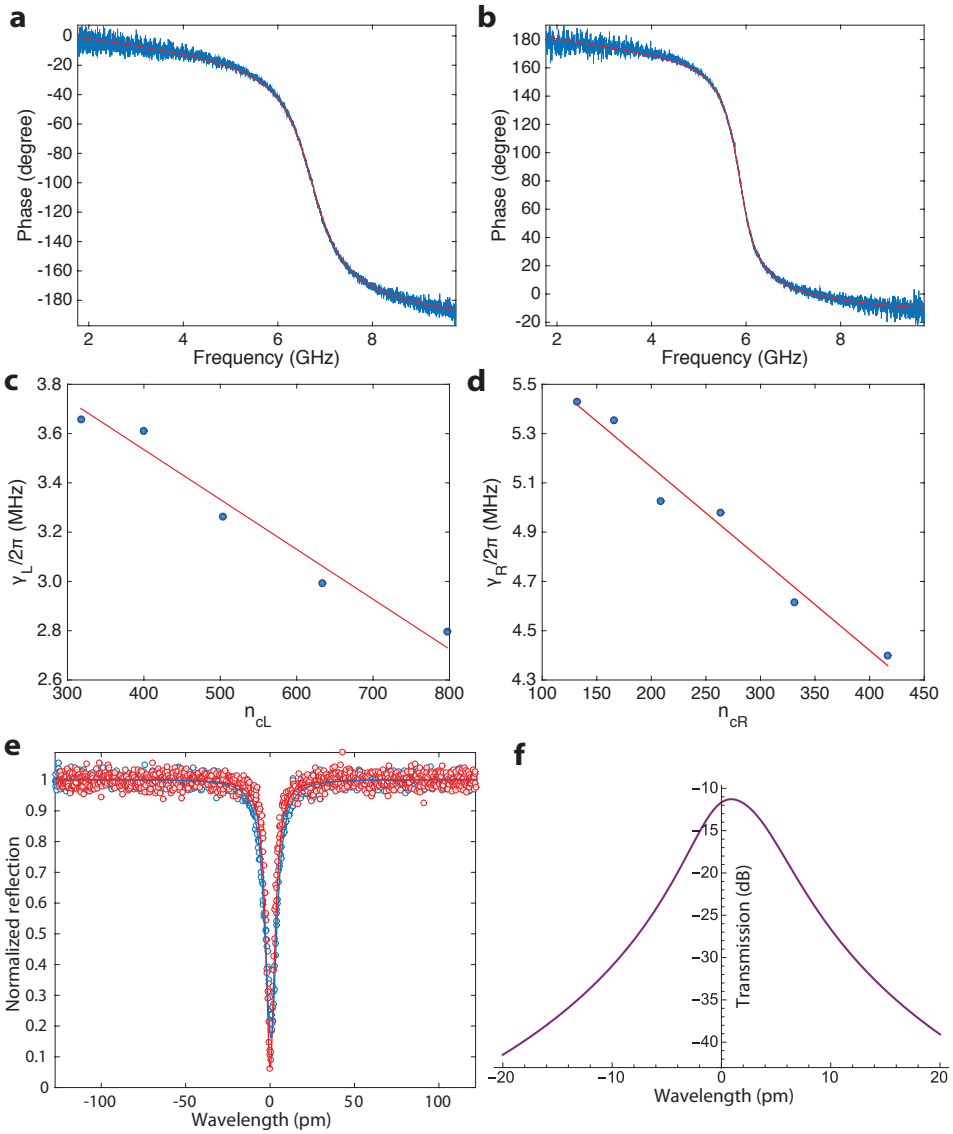

FIG. S2. **a**, Left optical cavity phase response as measured by scanning the probe signal across the cavity resonance with weak blue-detuned pump. **b**, Same as in **a** for the right optical cavity. **c**, Measured back-action modified mechanical linewidth versus intra-cavity pump photon number for the left optical cavity. Here only left cavity pump beam is applied, and the pump is tuned to the upper motional sideband of the cavity (blue-detuned with $\Delta = +\omega_{\mathrm{mL}}$). **d**, Same as in **c** for the right-side cavity and right-side pump. Measurements in **a-d** were performed prior to nano-oxidation tuning. **e** Measured (circles) and theoretical (solid curves) optical reflection spectra using a left-cavity (blue) and right-cavity (red) optical pump. These measurements are taken after nano-oxidation and the theoretical calculation includes the fit coupling ($J/2\pi = 110$ MHz) between the left and right optical cavity modes and a splitting between the uncoupled modes. The wavelength origin is taken to correspond to the right optical cavity resonance. **f** Calculated optical transmission power from one optical port to the other of an optical probe signal near resonance of the coupled optical cavity modes. Here there is no pump beam, and so no coupling to phonons. The parameters of the optical cavity modes are taken from the fit to the measured optical reflection spectra in **e**.

the mechanical cavity modes $M_{\mathrm{L(R)}}$ versus optical pumping power. In Fig. S2c the left cavity was pumped with a blue detuning $\Delta = +\omega_{\mathrm{mL}}$; in Fig. S2d the right cavity was pumped with a blue detuning of $\Delta = +\omega_{\mathrm{mR}}$. By fitting the measured data with formula $\gamma = \gamma_{\mathrm{i}} - 4g_0^2 n_c/\kappa$ (n_c corresponding to the intra-cavity photon number determined from the $O_{\mathrm{L(R)}}$ measured cavity properties), we obtain $g_{0,\mathrm{L(R)}}/2\pi = 0.76$ (0.84) MHz and $\gamma_{\mathrm{iL(R)}}/2\pi = 4.3$ (5.9)MHz for the left (right) localized cavity modes.

The optical (J) and mechanical (V) hopping rates between the two optomechanical cavities via the connecting waveguide are determined from a global fitting using Eq. (1) of the main text for the group of measured transmission coefficient ratio curves in Figs. 3c and 3d with varying Φ_{B}. The intra-cavity cavity photon number, optomechanical

coupling rates and intrinsic mechanical decay rates are all taken as fixed and equal to the independently measured values as described above.

With the fit value of J from forward and reverse transmission measurements versus $\Phi_{\rm B}$, and the measured cavity coupling rates (κ, $\kappa_{\rm i}$) from the left and right optical cavity modes prior to nano-oxidation tuning, we fit the measured optical reflection spectra of the two weakly coupled optical cavity modes after nano-oxidation. This allows us to determine the uncoupled left and right optical cavity mode frequencies. The measured and fit spectra as measured from the left and right cavities are shown in Fig. S2e. As noted earlier, the measured spectra after nano-oxidation are still predominantly given by uncoupled left and right cavity modes. Based on the theoretical fit to the measured optical reflection spectra, we also calculate the transmission of an optical probe signal through the optomechanical circuit in the absence of a pump beam (i.e., no coupling to phonons, just pure optical transmission)

$$\eta = \frac{J\sqrt{\kappa_{\rm eL}\kappa_{\rm eR}}}{|J^2 + \kappa_{\rm L}\kappa_{\rm R}/4 - (\omega-\omega_{\rm cL})(\omega-\omega_{\rm cR}) - i\kappa_{\rm L}(\omega-\omega_{\rm cL})/2 - i\kappa_{\rm R}(\omega-\omega_{\rm cR})/2|}. \tag{S2}$$

Fig. S2f shows the numerical result, and the minimum insertion loss for transmission from one port to the other port is found to be about 11 dB for a probe signal frequency in between the two cavity resonances. This is the estimated port-to-port optical transmission efficiency in absence of optomechanical amplification.

II. THEORY OF OPTICAL NONRECIPROCITY

A. Input-output formula

We provide theoretical analysis of optical nonreciprocity in the coupled optomechanical cavity system. We first consider the case with two optical and two mechanical cavity modes. The Hamiltonian of this system can thus be written down as follows,

$$\begin{aligned}\hat{H} = &\sum_{k=L,R}\hbar\omega_{ck}\hat{a}_k^\dagger\hat{a}_k + J(\hat{a}_L^\dagger\hat{a}_R + \hat{a}_L\hat{a}_R^\dagger) + \sum_{k=L,R}\hbar\omega_{mk}\hat{b}_k^\dagger\hat{b}_k + V(\hat{b}_L^\dagger\hat{b}_R + \hat{b}_L\hat{b}_R^\dagger)\\ &+ \sum_{k=L,R}\hbar g_{0k}(\hat{b}_k^\dagger + \hat{b}_k)\hat{a}_k^\dagger\hat{a}_k + \sum_{k=L,R} i\hbar\sqrt{\kappa_{ek}}\alpha_{pk}e^{-i\omega_{pk}t-i\phi_k}(\hat{a}_k - \hat{a}_k^\dagger),\end{aligned} \tag{S3}$$

where J and V are the waveguide mediated optical and mechanical coupling strength (we gauged out the phase of J and V and take both of them to be real), and the last two terms are the optical driving fields (pumps) which have the same frequency and correlated phases. We consider the situation where the optical cavities are nearly degenerate, i.e., $\omega_{cL} \simeq \omega_{cR} \equiv \omega_{\rm c}$ and both optomechanical systems are driven with a blue-detuned laser ($\omega_{pk} = \omega_{\rm c} + \omega_{mk}$). We perform a displacement transformation $\hat{a}_k = \alpha_k + \hat{d}_k$, separating the classical steady state amplitude of the local optical cavity field from its fluctuations. With this we can linearize the optomechanical interaction in the Hamiltonian of Eq. S3 in the usual manner. Assuming the good cavity limit (sideband resolved, $\omega_{mk} \gg \kappa_k$), we apply a rotating wave approximation and obtain for the equations of motions ($\hbar = 1$)

$$\begin{aligned}\frac{d}{dt}\hat{d}_L &= \left(i\Delta_L - \frac{\kappa_L}{2}\right)\hat{d}_L - \sqrt{\kappa_{eL}}\hat{d}_{L,\rm in} - \sqrt{\kappa_{iL}}\hat{\xi}_{L,\rm in} - iJ\hat{d}_R - iG_L\hat{b}_L^\dagger e^{i\phi_L},\\ \frac{d}{dt}\hat{d}_R &= \left(i\Delta_R - \frac{\kappa_R}{2}\right)\hat{d}_R - \sqrt{\kappa_{eR}}\hat{d}_{R,\rm in} - \sqrt{\kappa_{iR}}\hat{\xi}_{R,\rm in} - iJ\hat{d}_L - iG_R\hat{b}_R^\dagger e^{i\phi_R},\\ \frac{d}{dt}\hat{b}_L &= -\left(i\omega_{\rm mL} + \frac{\gamma_{\rm iL}}{2}\right)\hat{b}_L - \sqrt{\gamma_{\rm iL}}\hat{b}_{L,\rm in} - iV\hat{b}_R - iG_L\hat{d}_L^\dagger e^{i\phi_L},\\ \frac{d}{dt}\hat{b}_R &= -\left(i\omega_{\rm mR} + \frac{\gamma_{\rm iR}}{2}\right)\hat{b}_R - \sqrt{\gamma_{\rm iR}}\hat{b}_{R,\rm in} - iV\hat{b}_L - iG_R\hat{d}_R^\dagger e^{i\phi_R},\end{aligned} \tag{S4}$$

with the total damping rates $\kappa_k = \kappa_{ek} + \kappa_{ik}$, the detunings $\Delta_k = \omega_{\rm p} - \omega_{ck}$ and the many-photon optomechanical couplings $G_k = g_{0k}\alpha_k$. The latter contains the steady state amplitude of the local optical cavity field $\alpha_k e^{i\phi_k}$, which is related to the pump amplitudes through

$$\alpha_{L(R)}e^{i\phi_{L(R)}} = \frac{(i\Delta_{R(L)} - \kappa_{R(L)}/2)\sqrt{\kappa_{eL(R)}}\alpha_{pL(R)}e^{-i\varphi_{L(R)}} + iJ\sqrt{\kappa_{eR(L)}}\alpha_{pR(L)}e^{-i\varphi_{R(L)}}}{(i\Delta_L - \kappa_{\rm L}/2)(i\Delta_R - \kappa_{\rm R}/2) + J^2}. \tag{S5}$$

We find the steady state amplitude is approximately $\sqrt{\kappa_{ek}}\alpha_{pk}e^{-i\varphi_k}/i\Delta_k$ under the condition $\Delta_k \approx \omega_{mk} \gg \kappa_k, J$, which means each cavity is effectively only driven by its own optical pump. Thus, each pump-enhanced optomechanical coupling and its phase can be independently controlled. The intrinsic noise operators $\hat{\xi}_{k,\mathrm{in}}$ and $\hat{b}_{k,\mathrm{in}}$ in the coupled mode equations S4 describe thermal and vacuum fluctuations impinging on the the cavities and the mechanical modes respectively. The associated noise of a possible input signal is described via $\hat{d}_{k,\mathrm{in}}$.

B. Elimination of mechanics and mechanically-mediated interactions

We perform a Fourier transform ($\hat{b}[\omega] \equiv \int \mathrm{d}t\, \hat{b}(t)e^{+i\omega t}$; $\hat{b}(t) \equiv \int \frac{\mathrm{d}\omega}{2\pi}\, \hat{b}[\omega]e^{-i\omega t}$) of the coupled mode equations Eqs. S4 and insert the resulting solution for $\hat{b}^\dagger_{L,R}[\omega]$ into the equations of the cavity operators. Ignoring the intrinsic noise terms $\hat{\xi}_{\mathrm{in,k}}$ and $\hat{b}_{\mathrm{in,k}}$ for the moment, we obtain for the cavity operators in frequency space ($\Phi_\mathrm{B} = \phi_L - \phi_R$)

$$\begin{aligned}\widetilde{\chi}^{-1}_{L,+}[\omega]\hat{d}_L[\omega] &= -\sqrt{\kappa_{eL}}\hat{d}_{L,\mathrm{in}}[\omega] - i\left(J - \Gamma_+[\omega]e^{+i\Phi_\mathrm{B}}\right)\hat{d}_R[\omega],\\ \widetilde{\chi}^{-1}_{R,+}[\omega]\hat{d}_R[\omega] &= -\sqrt{\kappa_{eR}}\hat{d}_{R,\mathrm{in}}[\omega] - i\left(J - \Gamma_+[\omega]e^{-i\Phi_\mathrm{B}}\right)\hat{d}_L[\omega],\end{aligned} \tag{S6}$$

with the modified susceptibility $\widetilde{\chi}^{-1}_{k,+}[\omega] = \left(-i(\omega+\Delta_k) + \frac{\kappa_k}{2} + i\Sigma_{k,+}[\omega]\right)$. The frequency dependent coupling $\Gamma_+[\omega]$ and the self-energy $\Sigma_{k,+}[\omega]$ are defined as

$$\Gamma_+[\omega] = \frac{VG_RG_L}{\left[-i(\omega+\omega_{\mathrm{mL}}) + \frac{\gamma_{\mathrm{iL}}}{2}\right]\left[(-i(\omega+\omega_{\mathrm{mR}}) + \frac{\gamma_{\mathrm{iR}}}{2}\right] + V^2}, \qquad \Sigma_{k,+}[\omega] = \frac{iG_k}{VG_{\bar{k}}}\left[-i(\omega+\omega_{m\bar{k}}) + \frac{\gamma_{i\bar{k}}}{2}\right]\Gamma_+[\omega], \tag{S7}$$

here the coupling $\Gamma_+[\omega]$ coincides with Eq. (2) of the main text. After eliminating the mechanical degrees of freedom, one finds both a "local" modification of each cavity (described by the self energy $\Sigma_{k,+}[\omega]$) and an induced coupling between the cavities. The self-energies lead to damping (or anti-damping) of each cavity resonance as well as a frequency shift of the resonance. Here the subscript + indicates blue-detuning ($\Delta_k = \omega_{pk} - \omega_\mathrm{c} \approx +\omega_{mk}$). The poles of the self energy read

$$\omega_\pm = -\frac{i}{4}\left(\gamma_{\mathrm{iL}} + \gamma_{\mathrm{iR}}\right) - \frac{1}{2}\left(\omega_{\mathrm{mL}} + \omega_{\mathrm{mR}}\right) \pm \sqrt{V^2 - \left[\frac{1}{4}\left(\gamma_{\mathrm{iL}} - \gamma_{\mathrm{iR}}\right) - \frac{i}{2}(\omega_{\mathrm{mL}} - \omega_{\mathrm{mR}})\right]^2}. \tag{S8}$$

The induced coupling has a coherent and a dissipative aspect. To illustrate this we separate the coupling into real and imaginary parts $\Gamma_+[\omega] \equiv \Gamma_{\mathrm{Re}}[\omega] + i\Gamma_{\Im}[\omega]$. The real and imaginary parts of this frequency-dependent coupling have completely different physical interpretations. We see this, by considering again the coupling terms in Eq. (S6). We have

$$\begin{aligned}\hat{d}_L[\omega] &\sim \left[-i\left(J - \Gamma_{\mathrm{Re}}[\omega]e^{+i\Phi_\mathrm{B}}\right) - \Gamma_{\Im}[\omega]e^{+i\Phi_\mathrm{B}}\right]\hat{d}_R[\omega] \equiv \left[-i\widetilde{J}\ [\omega] - \Gamma_{\Im}[\omega]e^{+i\Phi_\mathrm{B}}\right]\hat{d}_R[\omega],\\ \hat{d}_R[\omega] &\sim \left[-i\left(J - \Gamma_{\mathrm{Re}}[\omega]e^{-i\Phi_\mathrm{B}}\right) - \Gamma_{\Im}[\omega]e^{-i\Phi_\mathrm{B}}\right]\hat{d}_L[\omega] \equiv \left[-i\widetilde{J}^*[\omega] - \Gamma_{\Im}[\omega]e^{-i\Phi_\mathrm{B}}\right]\hat{d}_L[\omega].\end{aligned} \tag{S9}$$

For the given frequency of interest, we see that the real part of the induced coupling is completely equivalent to having a Hamiltonian, coherent tunneling term between the cavities; we can absorb it into a redefinition of the coherent hopping strength J, i.e., $J \to \widetilde{J}[\omega]$. In contrast, the coupling mediated by the imaginary part $\Gamma_{\Im}[\omega]$ *is not* equivalent to some effective coherent tunneling interaction between the cavities, i.e., the $\Gamma_{\Im}[\omega]$ terms in $\hat{d}_L$ and $\hat{d}_R$ Eqs.(S9) cannot be incorporated into a definition of J. The terms involving $\Gamma_{\Im}[\omega]$ instead represent a *dissipative* coupling between the two cavities mediated by the mechanics. Such dissipative interactions (if we ignore their frequency dependence) can be obtained in a master equation formalism via an effective Lindblad dissipator of the form $2\Gamma_{\Im}\mathcal{L}\left[d^\dagger_L + e^{-i\Delta\phi}d^\dagger_R\right]$, where $\mathcal{L}[\hat{o}]\hat{\rho} = \hat{o}\hat{\rho}\hat{o}^\dagger - 1/2\hat{o}^\dagger\hat{o}\hat{\rho} - 1/2\hat{\rho}\hat{o}^\dagger\hat{o}$ is the standard Lindblad superoperator.

C. Directionality by balancing coherent and dissipative interactions

The dissipative coupling is crucial for directionality: by balancing the dissipative interaction against the coherent interaction we obtain a nonreciprocal system (following the general recipe outlined in Ref.[1]). For example, if we aim for a directional transport from the left to the right cavity, we want to decouple the left cavity from the right

cavity (while still having the right cavity influenced by the left cavity). This is accomplished by balancing coherent and dissipative interactions, i.e.,

$$\widetilde{J}[\omega] \stackrel{!}{=} i\Gamma_{\Im}[\omega]e^{i\Phi_{\mathrm{B}}}, \tag{S10}$$

in which case the coupling from the left to right cavity vanishes, cf. Eq. (S9), and we obtain a unidirectional coupling where the right cavity is driven by the left cavity but not vice versa. Crucially, this would not be possible without the dissipative interaction, i.e., we need $\Gamma_{\Im}[\omega] \neq 0$. Note, for the situation that $\Gamma_{\Im}[\omega] = 0$, i.e., $\gamma_{ik} = 0$, but finite Φ_{B}, we still obtain a directional dependent phase. However, to use this as the basic for nonreciprocal transmission additional interference processes have to implemented.

The directionality condition Eq. (S10) can be reformulated in terms of the original J and the phase difference Φ_{B} as used in Eq. (S6). This translates to the condition

$$J = |\Gamma_+[\omega]|\,, \qquad \Phi_{\mathrm{B}} = -\arg(\Gamma_+[\omega]), \tag{S11}$$

where we still aim for unidirectional behavior from left to right. For the case of a purely real coupling $\Gamma_+[\omega] = \Gamma_{\mathrm{Re}}[\omega]$ these conditions could still be satisfied, i.e., for $\Phi_{\mathrm{B}} = 0$ and $\Gamma_{\mathrm{Re}}[\omega] = J$. However, this means that there is effectively no coupling between the cavities, and thus no forward transport either. Note, that a sign change in $\arg(\Gamma_+[\omega])$ would lead to the opposite situation, where the propagation direction would be from right to left.

In general, the directionality balancing condition obtained here is frequency dependent, for the simple reason that the mechanically-mediated cavity-cavity coupling is frequency-dependent. If we could somehow fulfill the directionality condition in Eq. (S11) at every frequency, the cavity output field operators would be given by (using the standard input-output relation $\hat{d}_{k,\mathrm{out}} = \hat{d}_{k,\mathrm{out}} + \sqrt{\kappa_{ek}}\hat{d}_k$)

$$\begin{aligned}
\hat{d}_{L,\mathrm{out}}[\omega] &= [1 - \kappa_{eL}\widetilde{\chi}_{L,+}[\omega]]\,\hat{d}_{L,\mathrm{in}}[\omega], \\
\hat{d}_{R,\mathrm{out}}[\omega] &= [1 - \kappa_{eR}\widetilde{\chi}_{R,+}[\omega]]\,\hat{d}_{R,\mathrm{in}}[\omega] - i\sqrt{\kappa_{eR}\kappa_{eL}}\widetilde{\chi}_{R,+}[\omega]\widetilde{\chi}_{L,+}[\omega]\,|\Gamma_+[\omega]|\left(e^{i2\arg(\Gamma_+[\omega])} - 1\right)\hat{d}_{L,\mathrm{in}}[\omega],
\end{aligned} \tag{S12}$$

where we neglected the noise contributions originating from the mechanical modes, i.e., the coupling to $\hat{b}_{n,\mathrm{in}}$ in Eq. (S6), and the intrinsic cavity noise $\xi_{\mathrm{in,k}}$ for simplicity. Here, we see again that the dissipative interaction is crucial as we need $\arg(\Gamma_+[\omega]) \neq n\pi, n \in \mathbb{Z}$, i.e., we need a finite imaginary part of $\Gamma_+[\omega]$.

The experimentally relevant situation is where dissipative and coherent interactions are only balanced at a single frequency (by appropriate tuning of phase and J). Achieving this condition close to the normal modes resonance frequencies is favorable given the resonantly-enhanced transmission. Enforcing directionality at $\omega = -\omega_{\mathrm{m}} \pm V$ for equal mechanical resonance frequencies, results in the directionality conditions

$$\omega_{\mathrm{mL}} = \omega_{\mathrm{mR}}: \qquad \Phi_{\mathrm{B}} = \mp\arctan\frac{2V\,(\gamma_{\mathrm{iL}} + \gamma_{\mathrm{iR}})}{\gamma_{\mathrm{iL}}\gamma_{\mathrm{iR}}}, \qquad J = \frac{VG_RG_L}{\sqrt{\frac{1}{4}V^2\,(\gamma_{\mathrm{iL}} + \gamma_{\mathrm{iR}})^2 + \frac{\gamma_{\mathrm{iL}}^2\gamma_{\mathrm{iR}}^2}{16}}}, \tag{S13}$$

where the upper (lower) sign in the phase difference Φ_{B} realizes directionality at $\omega = -\omega_{\mathrm{m}} + V(-\omega_{\mathrm{m}} - V)$. Directionality here means that an input signal injected on the left cavity is transmitted to the right cavity, whereas the backward propagation path, i.e., from right to left, is blocked.

On the other side, if we assume identical bare mechanical damping of the mechanical modes ($\gamma_{\mathrm{iL}} = \gamma_{\mathrm{iR}} = \gamma_{\mathrm{i}}$), but unequal bare mechanical frequencies ($\omega_{\mathrm{mL}} \neq \omega_{\mathrm{mR}}$), then we find that at the frequencies of the hybridized mechanical modes $\Omega_\pm = -\frac{1}{2}\,(\omega_{\mathrm{mL}} + \omega_{\mathrm{mR}}) \pm \sqrt{V^2 + \frac{1}{4}(\omega_{\mathrm{mL}} - \omega_{\mathrm{mR}})^2}$ the directionality condition is modified to

$$\gamma_{\mathrm{iL}} = \gamma_{\mathrm{iR}}: \qquad \Phi_{\mathrm{B}} = \mp\arctan\frac{4\sqrt{V^2 + \frac{1}{4}(\omega_{\mathrm{mL}} - \omega_{\mathrm{mR}})^2}}{\gamma}, \qquad J = \frac{VG_LG_R}{\gamma\sqrt{V^2 + \frac{\gamma^2}{16} + \frac{1}{4}(\omega_{\mathrm{mL}} - \omega_{\mathrm{mR}})^2}}. \tag{S14}$$

where the upper (lower) sign in the phase difference Φ_{B} realizes directionality at $\omega = \Omega_{+(-)}$. The directionality conditions for a perfectly symmetric device, i.e., for equal mechanical resonance frequencies (ω_{m}) and decay rates (γ), can simply be read off from either Eq. S14 or Eq. S13.

D. Nonreciprocal optical transmission: two blue detuned pumps

From the equations for the cavity operators in Eqs. S6 we can calculate the transmission coefficients via input/output theory. Note, that although Eqs. S6 are formulated on the basis of noise operators, they as well describe the dynamics of the cavity field amplitudes d_k around their steady state solution. The right transmission coefficient $T_{\mathrm{L}\to\mathrm{R}} \equiv d_{R,\mathrm{out}}/d_{L,\mathrm{in}}$ and left transmission coefficient $T_{\mathrm{R}\to\mathrm{L}} \equiv d_{L,\mathrm{out}}/d_{R,\mathrm{in}}$ are given by

$$T_{R\leftrightarrows L}[\omega] = \frac{i\sqrt{\kappa_{\mathrm{eL}}\kappa_{\mathrm{eR}}}\left[J-\Gamma_+[\omega]e^{\mp i\Phi_{\mathrm{B}}}\right]}{\widetilde{\chi}_L^{-1}[\omega]\widetilde{\chi}_R^{-1}[\omega]+[\Gamma_+[\omega]^2+J^2-2\Gamma_+[\omega]J\cos(\phi)]} \equiv A_+[\omega]\left[J-\Gamma_+[\omega]e^{\mp i\Phi_{\mathrm{B}}}\right], \tag{S15}$$

with the modified susceptibilities $\widetilde{\chi}_k[\omega]$ as defined after Eq. (S6). The prefactor $A_+[\omega]$ is the same for both transmission amplitudes, it accounts for the mechanically-induced back-action on the optical cavities, cf. main text after Eq. (2). Note, that the corresponding prefactor for two red-detuned pumps is simply $A_-[\omega] = -A_+^*[-\omega]$.

We now assume a completely symmetric pair of mechanical cavities ($\omega_{\mathrm{mL}} = \omega_{\mathrm{mR}} = \omega_{\mathrm{m}}$ and $\gamma_{\mathrm{iL}} = \gamma_{\mathrm{iR}} = \gamma_{\mathrm{i}}$) and apply the corresponding directionality direction for symmetric parameters, cf. Eq. S14 or Eq. S13. The transmission coefficient for the through direction ($\to$) under these conditions of perfect nonreciprocity is given by,

$$T_{\to}[-\omega_{\mathrm{m}}\pm V] = \sqrt{\frac{\kappa_{\mathrm{eL}}\kappa_{\mathrm{eR}}}{\kappa_R\kappa_L}}\sqrt{\frac{1\pm i\frac{\gamma_{\mathrm{i}}}{4V}}{1\mp i\frac{\gamma_{\mathrm{i}}}{4V}}}\frac{8i\sqrt{\mathcal{C}_L\mathcal{C}_R}}{\left[\mathcal{C}_L\left(1\pm i\frac{\gamma_i}{2V}\right)-\left(1\mp i\frac{2V}{\kappa_L}\right)\left(2\pm i\frac{\gamma_i}{2V}\right)\right]\left[\mathcal{C}_R\left(1\pm i\frac{\gamma_i}{2V}\right)-\left(1\mp i\frac{2V}{\kappa_R}\right)\left(2\pm i\frac{\gamma_i}{2V}\right)\right]}, \tag{S16}$$

introducing the single cavity cooperativity $C_k \equiv 4G_k^2/\gamma_{\mathrm{i}}\kappa_k$. Considering as well symmetric optical cavities ($\kappa_{\mathrm{eL}} = \kappa_{\mathrm{eR}} = \kappa_{\mathrm{e}}$; $\kappa_{\mathrm{L}} = \kappa_{\mathrm{R}} = \kappa$) with symmetric optical pumping ($G_{\mathrm{L}} = G_{\mathrm{R}} = G$) the transmission coefficient simplifies to

$$T_{\to}[-\omega_{\mathrm{m}}\pm V] \overset{V\ll\kappa}{\simeq} \frac{8i\mathcal{C}\frac{\kappa_e}{\kappa}}{\left[2-\mathcal{C}\pm i\frac{\gamma_{\mathrm{i}}}{2V}(1-\mathcal{C})\right]^2}, \tag{S17}$$

with $C \equiv 4G^2/\gamma_{\mathrm{i}}\kappa$ and under the realistic assumption that the hopping rate V is much lower than the cavity decay rate κ. Here we work with blue-detuned pumping of both optical cavities ($\Delta \approx +\omega_{\mathrm{m}}$), which results in parametric amplification of each of the left and right mechanical modes and leads to amplification of the optical probe signal. This becomes apparent for the situation that the mechanical hopping rate is much faster than the intrinsic mechanical decay rate ($V/\gamma_{\mathrm{i}} \gg 1$). In this case the gain diverges for $\mathcal{C} \to 2$ (this is twice as large as for a single cavity instability because the mechanical modes are hybridized and thus the effective optomechanical coupling from the left or right optical cavity is reduced by a factor of $\sqrt{2}$, hence the cooperativity by a factor of 2). Note, for the situation $V/\gamma_{\mathrm{i}} \gg 1$, the directionality conditions at the hybridized mechanical modes $\omega = -\omega_{\mathrm{m}} \pm V$ simplifies to $J \simeq G_{\mathrm{L}}G_{\mathrm{R}}/\gamma_{\mathrm{i}}$ and $\Phi_{\mathrm{B}} \to \mp\pi/2$.

E. Nonreciprocal optical transmission: two red detuned pumps

The analysis for the the case of two red detuned pumps is similar to the blue-detuned case. The cavity operators in Eq.(S4) couple now to the mechanical lowering operators $\hat{b}_k$ and vice versa, while the detuning between the cavity resonances and the external pump tones yields $\Delta_k = -\omega_{mk}$. The ratio of transmission coefficients is found to be given by the following expression

$$\frac{T_{\mathrm{L}\to\mathrm{R}}}{T_{\mathrm{R}\to\mathrm{L}}} = \frac{J-\Gamma_-[\omega]e^{-i\Phi_{\mathrm{B}}}}{J-\Gamma_-[\omega]e^{+i\Phi_{\mathrm{B}}}} = \frac{J-\frac{VG_LG_R}{\left[-i(\omega-\omega_{\mathrm{mL}})+\frac{\gamma_{\mathrm{iL}}}{2}\right]\left[-i(\omega-\omega_{\mathrm{mR}})+\frac{\gamma_{\mathrm{iR}}}{2}\right]+V^2}e^{-i\Phi_{\mathrm{B}}}}{J-\frac{VG_LG_R}{\left[-i(\omega-\omega_{\mathrm{mL}})+\frac{\gamma_{\mathrm{iL}}}{2}\right]\left[-i(\omega-\omega_{\mathrm{mR}})+\frac{\gamma_{\mathrm{iR}}}{2}\right]+V^2}e^{+i\Phi_{\mathrm{B}}}} \tag{S18}$$

where we have $\Gamma_-[\omega] = \Gamma_+^*[-\omega]$, thus the ratio $|T_{\mathrm{L}\to\mathrm{R}}/T_{\mathrm{R}\to\mathrm{L}}|$ is the same for blue and red detuned pumps evaluated at corresponding frequencies. The reason for this is that the transmission is either amplified or suppressed simultaneously for both directions and thus their ratio stay unchanged. Comparing to the blue detuned case, the perfect nonreciprocity condition remains the same in the red detuned case, while the transmission coefficient for the through direction the

hybridized mechanical modes $\Omega_\pm = \omega_\mathrm{m} \pm V$ is given by (assuming $\omega_\mathrm{mL} = \omega_\mathrm{mR}$, $\gamma_\mathrm{iL} = \gamma_\mathrm{iR} = \gamma_\mathrm{i}$ and $V \ll \kappa_k$)

$$T_{\rightarrow}[\omega_\mathrm{m} \pm V] \simeq \sqrt{\frac{\kappa_\mathrm{eL}\kappa_\mathrm{eR}}{\kappa_R\kappa_L}} \frac{8i\sqrt{\mathcal{C}_L\mathcal{C}_R}}{\left[\mathcal{C}_L + 2 \pm i\frac{\gamma_\mathrm{i}}{2V}\left(\mathcal{C}_L+1\right)\right]\left[\mathcal{C}_R + 2 \pm i\frac{\gamma_\mathrm{i}}{2V}\left(\mathcal{C}_R+1\right)\right]}. \tag{S19}$$

From Eq. S19, we note in general an attenuated transmission for the red detuned case as $T_{\rightarrow} \leq \sqrt{\kappa_\mathrm{eL}\kappa_\mathrm{eR}/(\kappa_\mathrm{L}\kappa_\mathrm{R})} < 1$. For the case of a fast hopping rate $V/\gamma_\mathrm{i} \gg 1$ equality is achieved when $\mathcal{C}_k = 2$ and/or $\kappa_k/2 = \frac{G_\mathrm{L}G_\mathrm{R}}{\gamma_\mathrm{i}}$. Comparing the latter to Eq. S13 we see the maximal through transmission efficiency is achieved when the optical cavity loss rate $\kappa_k/2$ is matched to the inter-cavity photon hopping rate J for both cavities (impedance matching condition).

F. Nonreciprocity associated with a single mechanical waveguide mode

In our optomechanical circuits, we also observed optical nonreciprocity with a single mechanical waveguide mode. In this case, the Hamiltonian describing the interaction between two optical cavity modes and one mechanical waveguide mode is given by,

$$\begin{aligned}\hat{H} = &\sum_{k=\mathrm{L,R}} \hbar\omega_{\mathrm{c},k}\hat{a}_k^\dagger\hat{a}_k + J(\hat{a}_\mathrm{L}^\dagger\hat{a}_\mathrm{R} + \hat{a}_\mathrm{L}\hat{a}_\mathrm{R}^\dagger) + \hbar\omega_{M_\mathrm{W}}\hat{b}_\mathrm{W}^\dagger\hat{b}_\mathrm{W} \\ &+ \sum_{k=\mathrm{L,R}} \hbar\left(g_{0,\mathrm{W}k}\hat{b}_\mathrm{W} + g_{0,\mathrm{W}k}^*\hat{b}_\mathrm{W}^\dagger\right)\hat{a}_k^\dagger\hat{a}_k + \sum_{k=\mathrm{L,R}} i\hbar\sqrt{\kappa_{\mathrm{e}k}}\alpha_{\mathrm{p}k}e^{-i\omega_\mathrm{p}t-i\phi_k}(\hat{a}_k - \hat{a}_k^\dagger).\end{aligned} \tag{S20}$$

Going through a similar calculation using coupled mode equations, we find that the ratio of right and left optical transmission coefficients is

$$\frac{T_{\mathrm{L}\rightarrow\mathrm{R}}}{T_{\mathrm{R}\rightarrow\mathrm{L}}} = \frac{J \pm i\frac{|G_\mathrm{WL}G_\mathrm{WR}|}{-i\left(\omega\pm\omega_{M_\mathrm{W}}\right)+\frac{\gamma_\mathrm{iW}}{2}}e^{-i(\Phi_\mathrm{B}\pm\Phi_W)}}{J \pm i\frac{|G_\mathrm{WL}G_\mathrm{WR}|}{-i\left(\omega\pm\omega_{M_\mathrm{W}}\right)+\frac{\gamma_\mathrm{iW}}{2}}e^{+i(\Phi_\mathrm{B}\pm\Phi_W)}}, \tag{S21}$$

where the upper (lower) sign corresponds to the blue (red) detuned case and $\Phi_W = \arg(G_\mathrm{WL}^*G_\mathrm{WR})$. The corresponding conditions for perfect directionality from left to right and at $\omega = \mp\omega_{M_\mathrm{W}}$ are

$$J = \frac{2|G_\mathrm{WL}G_\mathrm{WR}|}{\gamma_\mathrm{iW}}, \qquad \Phi_\mathrm{B} = \pm\frac{\pi}{2} \mp \Phi_W. \tag{S22}$$

This in turn leads to the transmission coefficients

$$T_{\rightarrow}[\mp\omega_{M_\mathrm{W}}] = \sqrt{\frac{\kappa_\mathrm{eL}\kappa_\mathrm{eR}}{\kappa_\mathrm{L}\kappa_\mathrm{R}}} \frac{4i\sqrt{\mathcal{C}_{WL}\mathcal{C}_{WR}}}{(\mathcal{C}_{WL} \mp 1)(\mathcal{C}_{WR} \mp 1)}. \tag{S23}$$

In the case of blue detuned tones an input signal is amplified and the corresponding gain increases for $\mathcal{C}_{Wk} \rightarrow 1$.

Note in Eq. S22 we included the phase of the product $G_\mathrm{WL}^*G_\mathrm{WR}$. This addition comes from the fact that we have already chosen definitions for the local cavity mode amplitudes ($a_\mathrm{L,R}$ and $b_\mathrm{L,R}$) such that the phase of the optomechanical couplings of the localized cavity modes – $G_\mathrm{L} \equiv |\alpha_\mathrm{L}|g_{0,\mathrm{L}}$ and $G_\mathrm{R} \equiv |\alpha_\mathrm{R}|g_{0,\mathrm{R}}$ – are both zero. With these same definitions for amplitudes a_L and a_R we are not then free to set the phases of *both* G_WL and G_WL to be zero; not at least for the same set of pump phases ϕ_L and ϕ_R chosen for the localized cavity mode coupling. A simple example helps to illustrate this. The mode M_W can be viewed as a hybridization between the localized left and right cavity modes and a delocalized waveguide mode [2]. Using perturbation theory, we have for the mechanical mode amplitude of the hybridized mode M_W,

$$b_\mathrm{W} = b_{\mathrm{W}'} + \frac{t_\mathrm{L}}{\omega_{M'_\mathrm{W}} - \omega_\mathrm{mL}}b_\mathrm{L} + \frac{t_\mathrm{R}}{\omega_{M'_\mathrm{W}} - \omega_\mathrm{mR}}b_\mathrm{R}, \tag{S24}$$

where $b_{\mathrm{W}'}$ is the unperturbed delocalized waveguide mode amplitude and $\omega_{M'_\mathrm{W}}$ is the unperturbed frequency of the delocalized waveguide mode. $t_{\mathrm{L(R)}}$ is the coupling coefficient between the delocalized waveguide mode and the localized cavity mode $M_{\mathrm{L(R)}}$. The phases of t_L and t_R are determined by the field distribution of the hybridized mode M_W in the left and right cavities, respectively, and cannot be (both) chosen arbitrarily . Using the mode decomposition of Eq. S24, we have that $\arg(g_{0,\mathrm{WL}}^*g_{0,\mathrm{WR}}) = \arg(t_\mathrm{L}^*t_\mathrm{R})$ as we have already chosen a local cavity mode amplitude basis

such that $\arg(g_{0,\mathrm{L}}) = \arg(g_{0,\mathrm{R}}) = 0$ and $\omega_{M'_\mathrm{W}} > \omega_{\mathrm{mL}}, \omega_{\mathrm{mR}}$ (this assumes of course that the left (right) optical cavity mode only couples to the portion of b_W which is due to b_L (b_R), which is a good approximation due to the fact that the optical cavities are in the far field of each other). Thus, by *simultaneously* measuring the flux-dependent transmission near the resonance of the localized mechanical cavity modes and the hybridized mechanical waveguide mode we can determine the $\arg(g^*_{0,\mathrm{WL}} g_{0,\mathrm{WR}})$ in this mode basis (see Fig. S4 for example). For the M_W mode in our experiment, we find $\arg(g^*_{0,\mathrm{WL}} g_{0,\mathrm{WR}}) \approx \pi$, which means for this hybridized mode and chosen localized cavity mode basis the mechanical motion in the left cavity as seen by the left cavity optical mode is approximately 180 degrees out of phase with the motion in the right cavity as seen by the right cavity optical mode.

III. DIRECTIONAL FLOW OF QUANTUM AND THERMAL NOISE

Besides the nonreciprocal optical signal transmission, the flow of quantum and thermal noise in the optomechanical circuit is directional. This is a natural consequence of the system's scattering matrix having a directional form; the scattering matrix determines both the transmission of coherent signals, as well as noise properties. To show this, we calculate the symmetrized output noise spectral density via

$$\bar{S}_{k,\mathrm{out}}[\omega] = \frac{1}{2}\int \frac{d\Omega}{2\pi} \left\langle \left\{ \hat{d}_{k,\mathrm{out}}[\omega], \hat{d}^\dagger_{k,\mathrm{out}}[\Omega] \right\} \right\rangle, \tag{S25}$$

defined in the standard manner [3]. The mechanical and optical noise operators introduced in Eqs. S4 have zero mean and satisfy the canonical correlation relations:

$$\langle \hat{o}_{k,\mathrm{in}}[\omega] \hat{o}^\dagger_{k',\mathrm{in}}[\Omega] \rangle = \langle o^\dagger_{k,\mathrm{in}}[\omega] o_{k',\mathrm{in}}[\Omega] \rangle + \delta_{k,k'}\delta(\omega+\Omega) = \left(n^{\mathrm{th}}_{o_k} + 1\right)\delta_{k,k'}\delta(\omega+\Omega), \qquad \hat{o}_{k,\mathrm{in}} = \hat{d}_{k,\mathrm{in}}, \hat{\xi}_{k,\mathrm{in}}, \hat{b}_{k,\mathrm{in}}. \tag{S26}$$

where $n^{\mathrm{th}}_{o_k}$ is the thermal occupation of each bath. In what follows, we assume that we have no thermal occupation of the optical field. This is justified as we work with a very high optical frequency.

Figure S3a-d depicts the output spectra for the situation that both pumps are blue detuned from the cavity by ω_m. Here we assumed equal mechanical frequencies $\omega_{\mathrm{mL}} = \omega_{\mathrm{mR}} = \omega_\mathrm{m}$ and work in a rotating frame where the uncoupled mechanical resonance frequencies are shifted to zero. The remaining parameters are as used in the experiment, i.e., we take $\gamma_{\mathrm{iL}}/2\pi = 4.3$ MHz, $\gamma_{\mathrm{iR}}/2\pi = 5.9$ MHz, $\kappa_\mathrm{L}/2\pi = 1.03$ GHz, $\kappa_\mathrm{R}/2\pi = 0.75$ GHz, $\kappa_{iL}/2\pi = 0.29$ GHz, $\kappa_{iR}/2\pi = 0.31$ GHz, $V/2\pi = 2.8$ MHz, $J/2\pi = 110$ MHz. The multiphoton couplings $G_\mathrm{L} = G_\mathrm{R}$ used in the calculation are determined from Eq. S13.

Figure S3a shows the result for zero temperature mechanical baths and a finite phase $\Phi_\mathrm{B} = 0.36\pi$ (determined from Eq. S13). As expected, the L and R output spectra are not identical: while each has a double-peaked structure (corresponding to the two normal mode resonances), the right output spectra $\bar{S}_{R,\mathrm{out}}[\omega]$ has the upper-frequency peak larger than the lower-frequency peak, while the situation is reversed for the left output spectra. This does not lead to any asymmetry in the total output photon number fluxes (i.e., integrated over all frequencies). It does however lead to an asymmetry in the energy fluxes (i.e., as the higher energy peak is bigger for the right output spectrum, and the low energy peak is bigger for the left spectrum). Thus, the "quantum heating" of zero-point fluctuations preferentially cause an energy flow to the right (rather than to the left) for this choice of phase.

It is also worth noting that if all dissipative rates are equal for the R and L cavities, then the L output spectrum is just the frequency-mirrored R output spectrum. The latter is visible in Fig. S3(c), where we plotted the output spectra for symmetric parameters, i.e., we set $\gamma_{\mathrm{iR}}/2\pi = \gamma_{\mathrm{iL}}/2\pi = 4.3$ MHz, $\kappa_\mathrm{R}/2\pi = \kappa_\mathrm{L}/2\pi = 1.03$ GHz, $\kappa_{iR}/2\pi = \kappa_{iL}/2\pi = 0.31$ GHz and $\Phi_\mathrm{B} = 0.38\pi$ (determined from Eq. S13 for the new γ_{iR}). However, having unequal decay rates, i.e., $\gamma_R \neq \gamma_L$ and $\kappa_R \neq \kappa_L$, leads to a slight asymmetry even if the phase is set to zero, i.e., $\Phi_\mathrm{B} = 0$, as visible in Fig.S3b. In Fig. S3g we plot the asymmetry $\bar{S}_{L,\mathrm{out}}[\omega] - \bar{S}_{R,\mathrm{out}}[\omega]$ for all the four cases corresponding to Fig. S3a-d.

For finite temperature, we find that the output spectrum has a roughly linear dependence on the mechanical bath temperature: $\bar{S}_{k,\mathrm{out}}(T) = c_k n^{\mathrm{th}} + \bar{S}_{k,\mathrm{out}}(0)$ (assuming $n^{\mathrm{th}}_{b_L} = n^{\mathrm{th}}_{b_R} \equiv n^{\mathrm{th}}$). This linear dependence is visible if we compare Fig. S3c,d and Fig. S3e,f, where the latter show the output noise spectra for $n^{\mathrm{th}} = 10$ with symmetric cavity parameters. Additionally, we also calculate the added noise quanta to the transmitted signal

$$\bar{n}_{k,\mathrm{add}}[\omega] \equiv \frac{\bar{S}_{k,\mathrm{out}}[\omega]}{|T_k[\omega]|^2} - \frac{1}{2}, \tag{S27}$$

where $\frac{1}{2}$ is the half quanta noise of the vacuum optical fields injected from the coupler. Fig.S3h shows the added noise for left-right propagation with $\Phi_\mathrm{B} = 0.36\pi$ (and asymmetric experimental cavity parameters). The mechanical baths n^{th} are varied as denoted in each graph. Even if the cavities and the mechanics are only driven by vacuum noise the

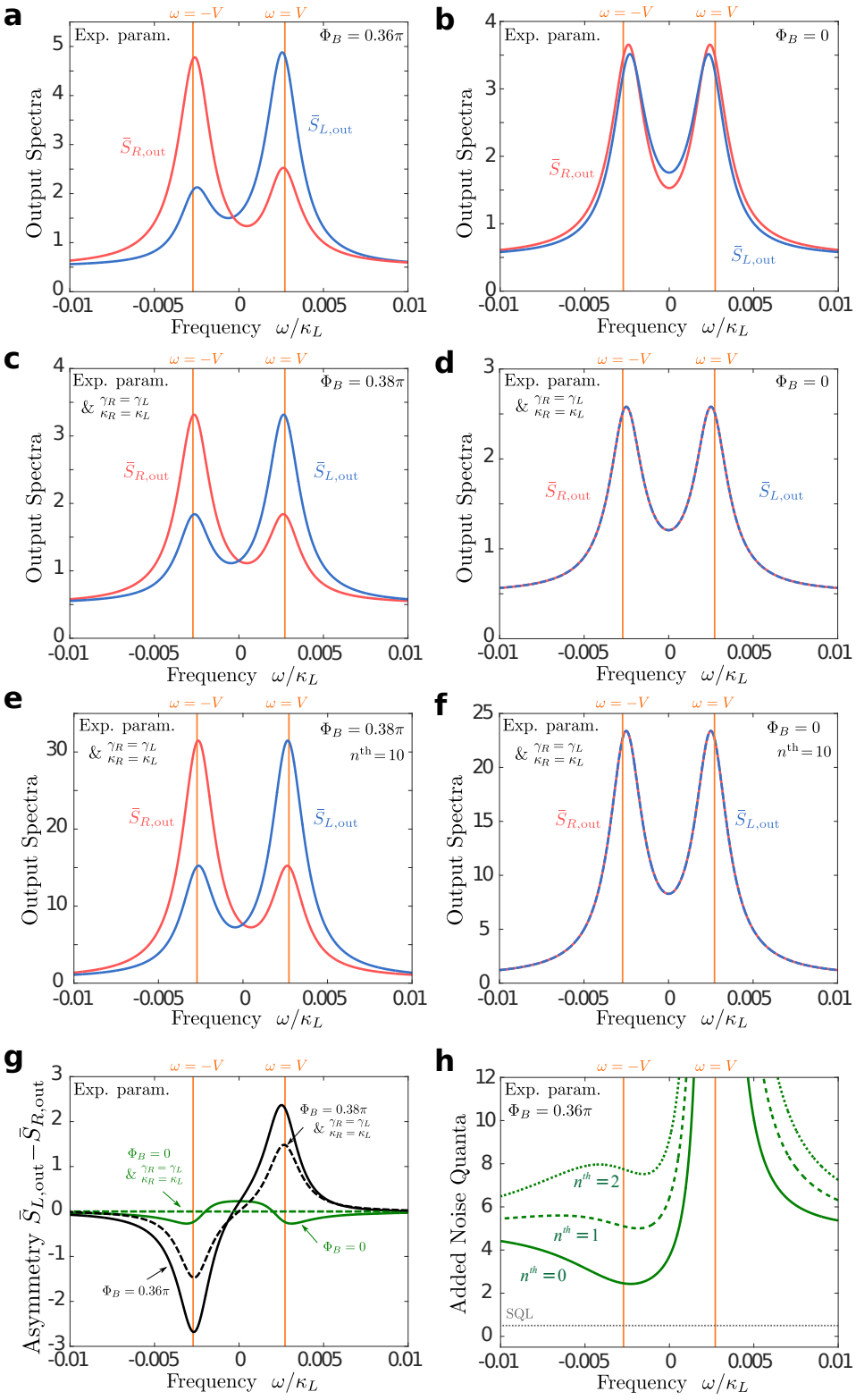

FIG. S3. **a-d** Output noise spectra at zero temperature for a set of parameters given in the text. **e-f** Output noise spectra at finite temperature with thermal phonon occupation of $n^{\rm th} = 10$. **g** Difference of the left and right output spectra for **a-d**. **h** Added noise for right-propagation of the signal signal.

standard quantum limit (SQL) of half a quanta is not achieved. This is due to the limited amount of gain achieved in the experiment, i.e., the transmission coefficient is not high enough to suppress the noise contributions. Moreover, even in the large gain limit the added noise would be roughly one quanta due to the finite amount of intrinsic optical cavity loss.

IV. RECIPROCAL CIRCUITS

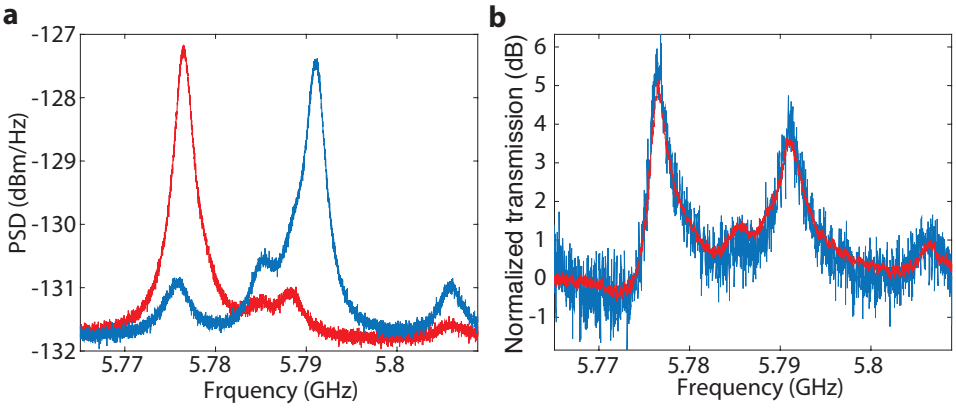

FIG. S4. Optical reciprocity in a circuit with large optical cavity coupling, J. **a** Mechanical spectra measured from the left (red) and right (blue) optical cavities. **b** Normalized optical signal power transmission coefficient for forward (red) and reverse (blue) optical signal propagation.

Realizing optical nonreciprocity in the optomechanical circuits studied in this work is not simple or easy as just creating a circuit with optical and mechanical coupling between two optomechanical cavities. One is limited by the practical realities of device power handling capability, finite optical and mechanical Q-factors, etc. As such, not all the circuits that were tested exhibited nonreciprocal transmission and amplification; the effects were too weak to observe in some circuits. This, however, was a useful test of our set-up as nonreciprocity could be effectively turned on and off by looking at different circuits with only slightly different parameters.

Eq. S14 sets the desired circuit parameters in order to achieve significant nonreciprocity, which for the optomechanical coupling, optical and mechanical Q-factors, and the power handling capabilities of the nanobeam cavities requires optical hopping rate between cavities to be less than $J/2\pi \approx 500$ MHz. Devices with larger coupling rates can simply not be pumped hard enough to satisfy $G_k \approx (J\gamma_{ik})^{1/2}$. To confirm this, here we show another optomechanical crystal circuit with bare cavity wavelengths of $\lambda_{L(R)} = 1535.051$ (1535.060) nm and inter-cavity photon hopping rate of $J/2\pi = 1.4$ GHz (more than ten times larger than the device studied in the main text). The mechanical spectra of this device as measured from both the left and right optical cavities is shown in Fig. S4a. Figure S4b shows the normalized transmission coefficient for forward and reverse optical signal propagation for a blue-detuned pump wavelength of $\lambda_p = 1534.99$ nm and synthetic flux of $\Phi_B = \pi/2$. Even at the largest pump powers ($P_p \approx 100$ μW; $n_c \approx 1.5 \times 10^3$) this device does not satisfy the condition of Eq. S14 due to the large J, resulting in nearly perfect reciprocity in the optical signal transmitted power. These measurements were performed on the exact same set-up as the circuit studied in the main text.

[1] A. Metelmann and A. Clerk, "Nonreciprocal photon transmission and amplification via reservoir engineering," *Phys. Rev. X*, vol. 5, p. 021025, 2015.
[2] K. Fang, M. H. Matheny, X. Luan, and O. Painter, "Optical transduction and routing of microwave phonons in cavity-optomechanical circuits," *Nature Photon.*, vol. 10, p. 489496, Jun. 2016.
[3] A. Clerk, M. Devoret, S. Girvin, F., Marquardt, and R. Schoelkopf, "Introduction to quantum noise, measurement, and amplification," *Rev. Mod. Phys.*, vol. 82, p. 1155, 2010.